Emergence of cortical inhibition by coordinated sensory–driven plasticity at distinct synaptic loci

Ramesh Chittajallu[*] and **John T.R. Isaac**[*]

Developmental Synaptic Plasticity Section, National Institute of Neurological Disorders and Stroke, National Institutes of Health, 35 Convent Drive, Bethesda, MD 20892, USA.

Abstract

Feed–forward GABAergic inhibition sets dendritic integration window thereby controlling timing and output in cortical circuits. However, it is unclear how feed–forward inhibitory circuits emerge, even though this is a critical step for neocortical development and function. Here we show that sensory–experience drives plasticity of the feed–forward inhibitory circuit in mouse layer 4 somatosensory "barrel" cortex in the second postnatal week by two distinct mechanisms. Firstly, sensory–experience selectively strengthens thalamocortical to feed–forward interneuron inputs via a presynaptic mechanism, but does not regulate other inhibitory circuit components. Secondly, experience drives a postsynaptic mechanism in which a down–regulation of a prominent thalamocortical NMDA EPSP in stellate cells regulates final expression of functional feed–forward inhibitory input. Thus, experience is required for specific, coordinated changes at thalamocortical synapses onto both inhibitory and excitatory neurons producing a circuit plasticity that results in maturation of functional feed–forward inhibition in layer 4.

Layer 4 of rodent somatosensory 'barrel' cortex is the major recipient of sensory input from the whiskers via the thalamus[1–3]. In the mature barrel cortex, thalamocortical transmission recruits parvalbumin-expressing, fast spiking interneurons that impart feed–forward inhibition onto layer IV excitatory stellate cells[4–9]. This truncates the thalamocortical response in stellate cells and sets a restricted time window within which synaptic input can be integrated[6]. The duration of this integration window is a critical feature for neocortical circuits, and primary sensory neocortex in particular, because it defines the temporal precision in neurons for faithful representation of sensory information encoded in thalamic synchrony[6,10–12]. Thus, appropriate development of feed–forward inhibition in layer 4 is an important prerequisite for sensory processing.

Recent work demonstrates that although fast spiking interneurons in layer 4 barrel cortex are present by P3, they are not incorporated into the network at this stage[7]. During subsequent development between postnatal day P3 – P9, these interneurons are recruited to the network through a series of coordinated events in the layer 4 circuit[7]. Many circuit features of barrel

[*]Correspondence: chittajallur@ninds.nih.gov, isaacj@ninds.nih.gov.

AUTHOR CONTRIBUTIONS

RC performed and analyzed the experiments. RC and JTRI designed the experiments and wrote the manuscript.

cortex development are dependent upon sensory experience[13,14] including, for example, receptive field formation in layer 4[15–18] and layer 2/3[19]. However, it remains unclear whether sensory experience is required for the developmental emergence of thalamocortical driven feed forward inhibition in layer 4 barrel cortex and, if so, the underlying synaptic mechanisms responsible. In addition, the role of sensory experience in the direct relationship between the developmental recruitment of feed–forward inhibition and the effect on integration window during postnatal developmental has also not been examined.

Here, we demonstrate that sensory–experience between P6–11 drives plasticity at thalamocortical inputs onto both inhibitory and excitatory neurons in layer 4 of the barrel cortex. These modifications involve different mechanisms despite being induced at synapses with the same presynaptic partner. At feed–forward interneurons there is an experience–dependent presynaptic change involving an increase in probability of release, whereas at stellate cells, experience drives a postsynaptic alteration involving a reduction of NMDA receptor–mediated EPSP. We propose that these coordinated, target–specific forms of experience–dependent synaptic plasticity combine to result in a narrow integration window in layer 4 stellate cells. Thus, our data highlight that sensory–experience during postnatal development plays an essential role in circuit formation that is a prerequisite for appropriate sensory information processing.

RESULTS

Emergence of feed–forward inhibition is sensory–driven

We made whole–cell patch–clamp recordings from stellate cells in layer 4 barrel cortex and elicited synaptic responses by stimulating ventrobasal thalamus (Fig. 1a). We calculated the GABA:AMPA ratio in stellate cells as a measure of the recruitment of feed–forward inhibition (see methods for details). In recordings from control mice (normal whisker experience) the GABA:AMPA ratio exhibited a developmental increase, consistent with previous work[7], and this ratio continued to increase at least until P11 (Fig. 1b; Supplementary Fig. 1a, b). Thus, thalamic recruitment of feed–forward inhibition was significantly larger at P9–11 compared to P6–8 (Fig. 1b, c) and was due to an increase of the disynaptic feed–forward IPSC amplitude relative to the monosynaptic EPSC (Supplementary Fig. 1c–f). We then assessed the effects of sensory–deprivation (i.e whisker–trimming; see methods for details) on the developmental recruitment of feed–forward inhibition. Whisker–trimming reduced feed–forward inhibition onto stellate cells at P9–11 (Fig. 1d, e). This effect was due to a smaller disynaptic IPSC relative to the EPSC in stellate cells (Supplementary Fig. 2). Interestingly, whisker–trimming produced a number of cells at P9–11 that did not receive any feed–forward IPSC (GABA:AMPA ratio = 0) a phenomenon that was never observed in P9–11 mice with normal whisker experience (Fig. 1d; Supplementary Fig. 2a, c). It must be noted, that whisker–trimming does not completely prevent the increase in G:A ratio observed between P6-8 and P9-11 (Fig. 1e). Thus, it is possible that part of the developmental increase in feed forward inhibition maybe independent of sensory experience. Another possibility, however, is that our deprivation protocol does not completely prevent sensory input. The whiskers were trimmed once a day and some whisker re–growth occurs in the 24–hour period between trimmings. This re–

growth may mediate some limited sensory driven input. Nevertheless, our data clearly demonstrate a role for sensory experience in mediating a developmental increase in feed forward inhibition.

Experience strengthens thalamic drive onto interneurons

The experience–dependent increase of GABA:AMPA ratio in layer 4 stellate cells could potentially arise from modifications of a number of components with the feed-forward inhibitory circuit. We therefore investigated the effects of whisker–trimming on this circuit using simultaneous recordings from feed–forward interneurons and stellate cells (Fig. 2a). Here, we defined a feed-forward interneuron as one that displays non-accommodating, fast-spiking action potential discharge with deep after-hyperpolarizations[7] (Fig. 2b). In addition the interneuron must receive a thalamocortical input and have a synaptic connection to a stellate cell which, in certain experiments, accounted for all of the disynaptic feed–forward inhibitory input elicited in the stellate cell at that given intensity of thalamic stimulation (Fig. 2c). We compared the size of thalamocortical EPSCs evoked in simultaneously recorded feed forward interneurons and stellate cells by stimulation of the same thalamic inputs. In slices from untrimmed littermate controls, the thalamocortical EPSC in feed–forward interneurons at P9–11 was approximately six times larger than in stellate cells (Fig. 2d–f), in agreement with previous studies[6,8,20]. However, in slices from whisker–trimmed mice the thalamocortical EPSC in feed–forward interneuron was only two times larger than in stellate cells (Fig. 2d–f). Thus, sensory experience drives a relative increase in the strength of the thalamocortical input to feed–forward interneurons compared to stellate cells.

These observed differences could be due to a decrease in thalamocortical input to feed–forward interneurons, an increase in the thalamocortical input to stellate cells or a combination of both. To investigate these possibilities and to also examine the underlying synaptic mechanisms responsible, we compared synaptic properties of responses evoked at putative single thalamocortical axons using minimal stimulation protocol (see methods for detail; Fig. 3a). Whisker–trimming caused an increase in failure rate of the thalamocortical input to feed-forward interneurons (Fig. 3b, c; $p < 0.01$). Although no effect on potency was observed (average EPSC amplitude excluding failures; Fig. 3d; $p = 0.14$), the whisker-trimming induced change in failure rate resulted in a significant reduction in mean EPSC amplitude (EPSC amplitude including failures; Fig. 3e; $p < 0.05$). We observed that whisker–trimming during the same developmental period had no effect on the thalamocortical input to stellate cells (Supplementary Fig. 4) demonstrating target-cell specificity in sensory-driven synaptic changes. We finally investigated short–term plasticity (measured as paired pulse ratio) at thalamocortical inputs onto feed–forward interneurons. These synapses exhibited paired pulse depression in untrimmed littermate controls whereas in whisker–trimmed mice there was marked paired pulse facilitation (Fig. 3f; $p < 0.05$). It must be noted that failure to reliably elicit action potentials in axons can contribute to failures when using minimal stimulation protocols and therefore we cannot exclude some contribution from such failures. However, the fact that we observed no changes in failure rate at thalamocortical to stellate cell inputs after whisker–trimming (Supplementary Fig. 3c; $p = 0.12$) combined with the previous observations that the same thalamocortical axon target both feed-forward interneurons and stellate cells[6,8] makes this an unlikely explanation of

our results. Also of note, is that an increase in connectivity could contribute to the experience-dependent strengthening but this is experimentally difficult to assess since we, and other groups, have found it impossible to record from pairs of thalamic and layer 4 neurons using conventional whole-cell recordings

We next investigated whether whisker experience affects synaptic transmission between feed–forward interneurons and stellate cells (Fig. 4a, b). In contrast to the thalamocortical input to feed–forward interneurons, whisker–trimming did not affect the probability (% connection = 57 and 60 in untrimmed and trimmed mice, respectively; n= 14 and 15; data not shown), the strength (p = 0.13; Fig. 4c) or short–term plasticity (p = 0.23 – 0.28 for all responses in train; Fig. 4d) of the feed–forward interneuron to stellate cell connection. In addition, no significant changes were noted in the decay kinetics of the unitary IPSC mediated by feed–forward interneurons at stellate cells (τ_{decay} of uIPSC = 5.5 ± 0.3 vs. 5.0 ± 0.36 in P9–11 trimmed and untrimmed littermates, respectively; p = 0.16, data not shown). We also showed that whisker–trimming had no significant effect on firing frequency, threshold, input resistance or membrane time constant of feed–forward interneurons (Supplementary Fig. 4).

Together, these findings indicate that sensory experience selectively modifies the thalamic input to feed–forward interneurons but does not influence thalamocortical inputs to stellate cells, intracortical aspects of the feed–forward inhibitory circuit or changes in intrinsic properties of interneurons. Thus, the developmental increase of the GABA:AMPA ratio observed[7] (Figure 1b) is mediated by a selective sensory-experience increase in thalamic recruitment of feed–forward interneuron via presynaptic changes that are, at least in part, due to a increase in release probability.

Developmental disparity between inhibition and truncation

Feed–forward inhibition in the mature layer 4 circuit shortens the integration window in stellate cells by truncating the thalamocortical postsynaptic potential (PSP) thus influencing dendritic integration and spike output of stellate cells[6] (Supplementary Fig. 5). Our experiments so far (Figs. 1–4) have analyzed the underlying synaptic mechanisms responsible for the developmental increase in feed–forward inhibitory input in layer 4 that occurs between P6 and P11. However these analyses do not address when during this developmental period the inhibitory input starts to have its functional impact by setting a narrow integration window in stellate cells as is observed in the mature circuit. We first assessed the extent of feed forward inhibition by measuring the GABA:AMPA ratio in each stellate cell (Fig. 5a) under voltage clamp during the P6–11 developmental period. We then switched to current–clamp mode to examine the resultant thalamocortical PSP time course at resting membrane potential (−60 to −75 mV; Fig. 5b) and used PSP half–width as a measure of the integration window. The mean peak amplitude of the thalamocortical PSPs in stellate cells was 7.4 ± 0.45 mV, corresponding to a mean membrane potential at the PSP peak of −65mV ± 0.63 mV (data not shown; n = 70). At P6–8, the PSP half width was significantly larger than at P9–11 (Fig. 5c, d). The relationship between GABA:AMPA ratio and PSP half width (Fig. 5e, f) showed that approximately 40% of P6–8 cells had GABA:AMPA ratios close to zero and exhibited PSPs with long time courses, consistent with the lack of feed–

forward inhibitory input. Approximately 35% P9–11 cells exhibited large GABA:AMPA ratios (> 4) and very rapid PSPs indicative of truncation via strong functional feed–forward inhibition. However, a significant proportion of stellate cells at P6–8 exhibited relatively large GABA:AMPA ratios, yet there was little shortening of the PSP. This phenomenon was particularly apparent for P6–8 cells with GABA:AMPA ratios of 2–4; in these cells feed–forward IPSC amplitude was up to four times greater than that of the EPSC, but there was relatively little truncation observed (Fig. 5b, e, f). At P9–11, however, cells with similar GABA:AMPA ratios of 2–4 did exhibit a marked shortening of the PSP (Fig. 5b, e, f).

These data demonstrate the presence of a disparity in the extent of thalamocortical PSP truncation between P6–8 and P9–11 stellate cells that exhibit essentially the same amount of feed-forward inhibition. The disparity suggests that there is an additional process in stellate cells that regulates the effectiveness of a given amount of feed–forward inhibition to produce truncation of the thalamocortical excitatory input at stellate cells. One possibility is that developmental changes in the intrinsic membrane properties of stellate cells contribute to the differences in the integration of feed–forward excitatory and inhibitory currents. However, in stellate cells displaying GABA:AMPA ratios of 2–4 there were no differences in input resistance (Supplementary Fig. 6a), whole–cell capacitance (Supplementary Fig. 6b), membrane time constant (Supplementary Fig. 6c) or resting membrane potential (Supplementary Fig. 6d) at the two age groups tested (P6–8 and P9–11). Another potential explanation is that the relative depolarizations mediated by thalamocortical stimulation are not equivalent between the two age groups thus leading to differences in the driving force for the $GABA_A$–receptor mediated feed–forward inhibitory current. However, there was no difference in PSP amplitude between the two groups excluding this explanation (Supplementary Fig. 6e). An additional possibility is a developmental change in the $GABA_A$ receptor subtype expressed postsynaptically on stellate cells that could contribute to differences in the integration of inhibitory currents. However, no difference in the time constant of IPSC decay was observed between the two groups (Supplementary Fig. 6f) also making this an unlikely explanation. Although we cannot fully rule out potential and differential contributions from sub–threshold active conductances, the above possibilities cannot underlie the disparity observed.

Presence of NMDA mediated EPSPs at resting potentials

We next investigated whether developmental changes in the properties of thalamocortical transmission onto stellate cells between P6–8 and P9–11 influence the integration window. Thalamocortical EPSCs recorded in voltage–clamp at a holding potential (Vh) of −70 mV in P6–8 stellate cells (Fig. 6a) exhibited a surprisingly large NMDA receptor–mediated current (Fig. 6b) that carried a similar amount of charge as the AMPA receptor–mediated component (Fig. 6c). Current–voltage (I–V) analysis of pharmacologically–isolated NMDA receptor–mediated EPSCs confirmed the existence of this prominent NMDA receptor– mediated component at close–to resting membrane potential values (−60 to −70 mV; Fig. 6d). Consistent with these data, in current–clamp mode a large thalamocortical NMDA receptor–mediated EPSP was recorded in stellate cells that could be evoked at resting membrane potential even in the absence of AMPA receptor–mediated depolarization (Fig. 6e, f). The size of the pharmacologically isolated NMDA receptor–mediated EPSC at resting

membrane potential values was significantly reduced during development. The NMDA EPSC peak at Vh of −70 mV as a percentage of NMDA EPSC peak at −30 mV (maximal inward NMDA current) was 41 % ± 4 % vs. 24 % ± 3 % for P6-8 and P9-11, respectively (data not shown; p< 0.05). In addition, the ratio of the NMDA and AMPA receptor–mediated components of the thalamocortical EPSC measured at −70 mV (see methods) at P9–11 was about half that observed at P6–8 (Fig. 6g). Since we see a decrease in the size of the NMDA–receptor component (P6–8 vs. P9–11 = 11.9 ± 1.25 vs. 5.7 ± 1.2 pA; p < 0.001; data not shown) but no significant difference in the size of the AMPA–receptor mediated component (P6–8 vs. P9–11 = 148 ± 10 vs. 146 ± 9 pA; p = 0.17; data not shown), the developmental decrease in the NMDA:AMPA ratio observed is due to a decrease in the contribution of the NMDA–receptor mediated component to thalamocortical synaptic transmission in stellate cells. The developmental shift in NMDA:AMPA ratio is also prominent between cells in the two age groups that have the same GABA:AMPA ratios (Fig. 6h; p < 0.01), in particular those with GABA:AMPA ratios between 2 and 4. Taken together, these data demonstrate the presence of a an NMDA receptor–mediated component that is significantly present at resting membrane potentials in stellate cells at P6–8 and is down–regulated over the next few days (P9-11).

NMDA component offsets feed–forward inhibitory truncation

The relatively slow NMDA receptor–mediated EPSP observed in stellate cells could prolong the PSP and therefore act in an opposite manner to feed forward inhibition with regard to the PSP ½ width. This could explain our previously noted discrepancy in the PSP ½ width between stellate cells at differing developmental stages that receive similar amounts of feed forward inhibitory input (see Figure 5f). We tested this possibility by investigating whether there is a correlation between the size of the NMDA receptor–mediated component of the thalamocortical EPSC (measured as the NMDA:AMPA ratio at a holding potential of −70 mV) and PSP half width for all stellate cells with a GABA:AMPA ratios of 2–4. Note that changes in the NMDA:AMPA ratio in this subset of stellate cells reflect differences in the contribution of the NMDA–receptor mediated component to thalamocortical synaptic transmission since we see a decrease in the NMDA–receptor component (P6–8 vs. P9–11 = 10.3 ± 2.6 vs. 4.7 ± 0.9 pA; n = 8 and 9, respectively; p < 0.01; data not shown) but no significant difference in the size of the AMPA–receptor mediated component (P6–8 vs. P9–11 = 135 ± 14 vs. 137 ± 19 pA; n = 8 and 9, respectively; p = 0.18; data not shown). A strong correlation was observed (r = 0.69; p < 0.01) showing that those cells with larger NMDA receptor–mediated components exhibit longer PSPs (Fig. 7b, c), even though the GABA:AMPA ratios (i.e the amount of feed forward inhibitory input) are similar (P6–8 vs. P9–11 = 2.84 ± 0.2 vs 2.69 ± 0.3; n = 8 and 9, respectively; p = 0.21).

We next examined the effects of acute NMDA–receptor blockade on PSP ½ width in stellate cells. For this experiment, the amount of feed–forward inhibitory transmission (i.e GABA:AMPA ratio) was first determined in voltage–clamp. Next in current–clamp mode in the same cells, PSPs were recorded before and in the presence of bath–applied NMDA–receptor antagonist D–APV (50 μM) and, in a final step, the presence of any GABA$_A$ receptor–mediated IPSP was tested by subsequent addition of gabazine (GBZ; 10 μM; while still in the presence of D–APV). In stellate cells exhibiting no feed–forward IPSC

(GABA:AMPA ratio = 0), application of D–APV caused a shortening of the PSP demonstrating the presence of an NMDA receptor–mediated component to thalamocortical transmission, as previously shown (Fig. 6). Subsequent addition of GBZ had no further effect on PSP half width confirming the lack of any functional feed–forward inhibition in these stellate cells (Fig. 7d, e, h). In stellate cells with high GABA:AMPA ratios (> 4) addition of D–APV had no effect on PSP half width, but addition of GBZ caused a marked prolongation of the PSP (Fig. 7d, f, h). This is consistent with strong truncation by feed–forward inhibition in these cells and a lack of influence of an NMDA receptor–mediated EPSP component on the PSP ½ width. For P6–8 cells in the critical 2–4 range of GABA:AMPA ratios, D–APV caused a large reduction in PSP half width and subsequent addition of GBZ + D–APV caused a prolongation of the PSP (Fig. 7d, g, h). Thus, NMDA receptor blockade in the P6–8 cells with GABA:AMPA ratios of 2–4 is sufficient to reveal a marked PSP truncation mediated by feed–forward inhibition. This demonstrates that the prominent NMDA receptor–mediated EPSP results in a relatively long PSP ½ width (~ 60 ms) even in the presence of significant feed forward inhibitory input in stellate cells. It is important to note that in these experiments the mean control PSP amplitude in stellate cells was 8.8 ± 0.9 mV that corresponded to a mean membrane potential at the depolarized peak of the PSP of -64 ± 1.3 mV (n=13). Note that D–APV or D–APV + GBZ did not cause any significant change in membrane potential in stellate cells (Supplementary Fig. 7a) excluding this as an alternative explanation to the effects of the drugs. D–APV caused a trend to a small depression of thalamocortical to feed–forward interneuron transmission (Supplemental Fig. 7b), thus excluding an effect of NMDA receptor blockade at the thalamocortical input to feed–forward interneuron as an explanation for the APV–mediated unmasking of feed–forward inhibition.

In further experiments, we also investigated the effects of blocking the feed forward inhibitory input in P6–8 stellate cells with a G:A ratio of 2–4 using local perfusion of GBZ. This blockade of feed forward inhibitory input caused a further prolongation of the PSP (Supplementary Fig. 8) resulting in PSP ½ width values similar to those observed in stellate cells exhibiting no feed forward inhibitory input but large NMDA component (i.e. GABA:AMPA ratio = 0; e.g. Figure 5f and 6i).

Thus, these data demonstrate that the prominent NMDA component present at P6–8 prolongs the PSP, whereas feed forward inhibitory input in the same cells independently acts to shorten the PSP. Thus, these two components driven by thalamocortical input interact with each other to influence the absolute PSP ½ width and hence set the integration window in stellate cells.

Sensory–experience reduces NMDA–receptor mediated offset

Our data shows that the developmental up–regulation of feed–forward inhibitory input combined with the down–regulation of the thalamocortical NMDA EPSP in stellate cells results in the emergence of marked PSP truncation by by P9–11. We next investigated whether experience also plays a role in modulating the interaction between the feed-forward inhibitory and the NMDA-receptor mediated inputs at stellate cells.

Consistent with a reduced feed–forward inhibition (Fig. 1d, e), whisker–trimming caused a significant increase in PSP half width (Fig. 8b–d) and in cells with GABA:AMPA ratios < 4 there was minimal PSP truncation similar to that observed in P6–8 stellate cells (Fig. 8e, f). When the relationship between PSP half width and NMDA:AMPA ratio (at HP = –70 mV) was analyzed, cells in the critical GABA:AMPA ratio range of 2–4 (from both whisker–trimmed and untrimmed littermates) showed a strong positive correlation (r = 0.65; p < 0.01) between amount of NMDA EPSC and PSP half width, but cells from the trimmed group consistently showed larger NMDA:AMPA and PSP half width values, with a distribution of values similar to those for P6–8 (Fig. 8g, h). These findings show that sensory experience plays a role in reducing the prolonging offset mediated by thalamocortical NMDA-receptor transmission thus resulting in smaller PSP ½ widths produced by a given amount of feed-forward inhibition.

DISCUSSION

Our current data demonstrate that whisker experience during development recruits feed-forward inhibition onto stellate cells in layer 4 barrel cortex by strengthening the thalamocortical input onto feed-forward interneurons. This occurs via a presynaptic mechanism involving an increase in release probability. For this increased feed-forward inhibitory input to effectively set a narrow integration window in stellate cells, we find that a second experience-dependent step occurs. At P6-8 thalamocortical inputs to stellate cells exhibit a remarkably large NMDA-receptor mediated EPSP at resting membrane potentials that prolongs the PSP and thus effectively offsets the truncation mediated by feed-forward inhibition. An experience-dependent down regulation of this component removes this offset allowing the feed forward inhibitory input to truncate the PSP resulting in a narrow integration window. Thus, sensory experience drives two distinct forms of developmental synaptic plasticity at thalamocortical inputs onto feed forward interneurons and stellate cells.

Sensory manipulations involving whisker deprivation/whisker sparing paradigms starting at P0 – P12 are known to profoundly affect the response properties of layer 4 neurons subsequently recorded in vivo in adult animals. In such studies whisker manipulations are typically chronic, lasting for many weeks, and result in increased spontaneous activity, increased whisker–evoked activity and an enlargement of receptive field in layer 4 excitatory neurons[15–18]. Intracortical inhibition in layer 4 is also altered by whisker manipulations as are the dynamics of the whisker–evoked responses of 'fast spiking units', presumed inhibitory interneurons[17]. Notably, the effects on the layer 4 circuit are not reversible, persisting if whiskers are allowed to re–grow from P30[15–18]. Thus, these studies point to a critical period of circuit maturation in layer 4 taking place during the first two postnatal weeks. Of particular relevance to the current work is the finding that intracortical inhibition and inhibitory interneuron response properties are altered with deprivation in the second postnatal week[16–18]. Moreover, these findings provide evidence that thalamocortical mechanisms, as those described in our current study, underlie such changes. Taken together with our data, this work suggests that experience–driven maturation of thalamocortical inputs to layer 4 during postnatal development plays a critical role in defining the mature response properties of both excitatory and inhibitory neurons in layer 4.

Previous work has highlighted a number of coordinated synaptic and cellular changes that underlie a rapid engagement of feed–forward interneurons during development of barrel cortex[7]. These include an increased thalamic drive to feed forward interneurons and an increased connectivity/synaptic strength between feed–forward interneuron and stellate cells[7]. Here, we show sensory experience during the same developmental period that alters thalamocortical drive to feed–forward interneurons, does not influence intracortical feed–forward interneuron to stellate cell connectivity or strength. Interestingly, in layer 4 visual cortex, intracortical connections from fast spiking interneurons onto glutamatergic principal cells undergo marked potentiation following two days of sensory deprivation[22]. However, in these studies sensory deprivation was initiated in older animals when functional inhibition had already been established. In addition, long–term whisker deprivation (for at least 20 days starting from the first postnatal week) results in feed–forward interneurons that fire action potentials less robustly[17,23]. Here, we observed no significant alterations in the passive membrane properties or intrinsic excitability of feed–forward interneurons. These observations taken together with our findings show that experience–driven plasticity of neural circuits is not uniform in nature across different neocortical regions and appears to be differentially impacted by the length and developmental timing of sensory deprivation.

The fact that sensory experience results in circuit changes at the thalamocortical input to feed–forward interneurons and stellate cells points to the involvement of activity–dependent synaptic plasticity. Indeed there is strong evidence for the idea that LTP and LTD underlies experience–dependent modification of cortical circuits in barrel[24,25] and visual cortices[22,26,27]. Thalamocortical synaptic transmission onto interneurons mediating feed–forward inhibition in layer 4 barrel cortex is mediated primarily by GluR2–lacking, Ca^{2+}–permeable (CP–) AMPA receptors [20]. In hippocampus, excitatory inputs onto interneurons with similar synaptic properties exhibit anti–Hebbian LTP that has a presynaptic locus of expression involving increase in the release probability[28,29]. This shares similarities with the synaptic mechanisms underlying the sensory experience–dependent recruitment of feed forward inhibition we describe here and therefore constitutes a potential candidate mechanism although a direct link remains to be proven.

Previous studies demonstrate sensory experience driven synaptic changes in NMDA–receptor expression in various sensory cortices[30–32]. Our results suggest that the NMDA receptor subtype expressed at thalamocortical synapses onto stellate cells in layer 4 barrel cortex at P6–8, exhibits a reduced voltage–dependent Mg^{2+} block. Furthermore, the sensory–mediated down–regulation is a key step in the emergence of thalamocortical PSP truncation in stellate cells. The presence of functional NMDA–receptor subunits that confer low Mg^{2+}–sensitivity have been identified in stellate cells [33–35]. Interestingly, the expression of these subunits has been shown to peak at the end of the first postnatal week[36–38], corresponding to the developmental period at which we observe significant NMDA-receptor mediated signaling around resting membrane potentials. Recent work shows that at developing hippocampal CA1 synapses, activity-dependent mechanisms exist that result in plasticity of NMDA-receptor expression via either removal or switching of subunits[39,40]. Similar mechanisms, driven by sensory experience, could serve to convert the relatively Mg^{2+} insensitive NMDA receptor to one that is effectively blocked by Mg^{2+} at resting membrane potentials during development. However, future work is required to

determine the subunit composition of the NMDA–receptor that offsets feed-forward inhibition and the exact synaptic mechanism(s) underlying its experience–dependent down–regulation.

The presence of distinct sensory–driven synaptic mechanisms highlighted in the current study raises the question: why the need for such tuning of feed–forward inhibition during development? Layer 4 barrel cortex contains a predominance of excitatory stellate cells that are highly interconnected in the mature circuit[41–43]. At the beginning of the second postnatal week, at the same time as feed–forward inhibition emerges, the connectivity of the stellate cell excitatory network increases rapidly (Ashby and Isaac, unpublished observations). We hypothesize that this rapidly developing excitatory network needs to be counterbalanced by a corresponding increase in functional feed–forward inhibition to maintain network excitability at a constant level. The mechanisms we describe here, which uses a change in feed–forward excitation to rapidly switch on feed–forward inhibition that is already in place, potentially provides an ideal process to enable coordinated developmental recruitment of balanced feed–forward inhibition. Moreover as layer 4 matures, the integration window, which is initially very large and promotes induction of long–term synaptic plasticity, needs to be shortened to provide the mature circuit with the necessary temporal precision to faithfully represent sensory input arriving from the whiskers. The underlying synaptic plasticity mechanisms described here thus achieve this important change to the circuit in response to sensory experience during a brief defined period of development.

METHODS

Electrophysiological recordings

Thalamocortical slices were prepared from P6 to P11 wild–type or GAD67:GFP knock–in[44] C57/Bl6 mouse pups[45,46] as approved by the US National Institute of Neurological Disorders and Stroke Animal Use and Care Committee. Whole cell voltage– and current–clamp recordings from layer 4 neurons were performed as described previously[7]. Thalamocortical EPSCs and EPSPs were evoked at a frequency of 0.1 Hz using a bipolar stimulating electrode placed in the ventrobasal thalamus. To evaluate the extent that thalamic stimulation recruits disynaptic feed–forward inhibition onto stellate cells, the ratio of the peak amplitude of the $GABA_A$–receptor mediated IPSC (measured at 0 mV) to the peak amplitude of the AMPA–receptor mediated EPSC (measured at −70 mV) was calculated and is termed the GABA:AMPA ratio. The stimulus intensity employed was the maximal intensity (typically 10–40 V) that resulted in a monosynaptic EPSC response in the stellate cell (i.e. no presence of recurrent activity). Firstly, this criterion ensured that any inhibition recorded in the stellate cells was exclusively feed–forward in nature. Secondly, this non–minimal level of stimulation also ensured that we could recruit feed–forward inhibition if it were present especially under experimental conditions in which this could be compromised i.e. sensory deprivation. NMDA:AMPA ratio was calculated by measuring the peak (AMPA) and tail (NMDA; 40–50 ms window after EPSC onset) currents of the thalamically–evoked EPSC in stellate cells at an holding potential of −70 mV. Current–voltage relationships for the NMDA–receptor mediated component of thalamocortical

synaptic transmission onto stellate cells were obtained in the presence of NBQX (20 μM) and picrotoxin (50 μM). For paired recordings a whole–cell recording from a GFP–positive interneuron in layer 4 barrel cortex was first obtained and then sequential whole cell recordings were made from neighboring stellate cells within a radius of 100 μm. Interneurons were classified as feed–forward if they received a monosynaptic excitatory input upon VB stimulation and were also synaptically connected to the subsequently recorded stellate cell. To test for connectivity to the stellate cell, the interneuron was brought to firing threshold by either synaptic stimulation in VB or by current injections of typically 300–1000 pA for 10 ms.

Minimal stimulation of thalamic inputs

Thalamic stimulation was adjusted until the lowest intensity was found (typically between 0.2V–4V) that stably elicited a combination of EPSCs (successes) and failures. Data was collected for at least 30 trials (at 0.1Hz) and in each trial paired pulse stimulation was employed. Potency was calculated as the mean EPSC peak amplitude excluding failures[21]. Mean unitary amplitude was calculated as the amplitude of all trails averaged together (EPSCs plus failures). Failure rate was calculated as number of failures/total number of trials. Paired pulse ratios was calculated as mean unitary EPSC amplitude of the second stimulus divided by mean EPSC peak amplitude of the first stimulus (S2/S1; stimuli given at 50 Hz).

Sensory deprivation protocol

Unilateral trimming of all whiskers from the right mystacial pad commenced on P5 until P9–11. During this period, trimming was performed every 24 h. In each litter about half of the pups were trimmed and the remainder were handled for a similar amount of time without trimming (untrimmed littermate controls). In all cases, thalamocortical slices were prepared such that they contained the barrel cortex of the left cerebral hemisphere. Recordings were interleaved between slices from whisker–trimmed mice and untrimmed littermates.

GABA$_A$–receptor antagonism via local perfusion

In certain experiments requiring absence of glutamate receptor antagonists, local perfusion of GBZ was performed because bath–application produced epileptiform activity. This was achieved using a patch pipette containing 50 μM GBZ connected to a picospritzer (PLI–100, Harvard Apparatus, MA) placed approximately 50–100 μm "up–stream" of the recording bath perfusion flow from the recorded cell. Local application was elicited during sweeps by a 50 ms pressure pulse that was delivered 40ms prior to electrical stimulation. Ejection of GBZ was monitored by additional inclusion of 10 μM fluoroscein in the perfusion pipette.

Statistics and graphical representation

Non–parametric statistical analyses using two–tailed Mann–Whitney U–test or the Kolmogorov–Smirnov test as appropriate. Statistical significance is indicated as * $P < 0.05$; **$P < 0.01$; ***$P < 0.001$. Box–and–whisker plots are constructed as follows; upper and lower limit of box indicates 75th and 25th percentile, respectively; line and circle within box

denotes the median and mean, respectively; Upper and lower limits of the capped lines indicate maximum and minimum values within the dataset, respectively.

Supplementary Material

Refer to Web version on PubMed Central for supplementary material.

ACKNOWLEDGEMENTS

REFERENCES

1. Woolsey TA, Van der Loos H. The structural organization of layer IV in the somatosensory region (SI) of mouse cerebral cortex. The description of a cortical field composed of discrete cytoarchitectonic units. Brain Res. 1970; 17:205–242. [PubMed: 4904874]

2. Bureau I, von Saint Paul F, Svoboda K. Interdigitated paralemniscal and lemniscal pathways in the mouse barrel cortex. PLoS Biol. 2006; 4:e382. [PubMed: 17121453]

3. Petreanu L, Mao T, Sternson SM, Svoboda K. The subcellular organization of neocortical excitatory connections. Nature. 2009; 457:1142–1145. [PubMed: 19151697]

4. Porter JT, Johnson CK, Agmon A. Diverse types of interneurons generate thalamus-evoked feedforward inhibition in the mouse barrel cortex. J Neurosci. 2001; 21:2699–2710. [PubMed: 11306623]

5. Swadlow HA. Thalamocortical control of feed-forward inhibition in awake somatosensory 'barrel' cortex. Philos Trans R Soc Lond B Biol Sci. 2002; 357:1717–1727. [PubMed: 12626006]

6. Gabernet L, Jadhav SP, Feldman DE, Carandini M, Scanziani M. Somatosensory integration controlled by dynamic thalamocortical feed-forward inhibition. Neuron. 2005; 48:315–327. [PubMed: 16242411]

7. Daw MI, Ashby MC, Isaac JT. Coordinated developmental recruitment of latent fast spiking interneurons in layer IV barrel cortex. Nat Neurosci. 2007; 10:453–461. [PubMed: 17351636]

8. Cruikshank SJ, Lewis TJ, Connors BW. Synaptic basis for intense thalamocortical activation of feedforward inhibitory cells in neocortex. Nat Neurosci. 2007; 10:462–468. [PubMed: 17334362]

9. Sun QQ, Huguenard JR, Prince DA. Barrel cortex microcircuits: thalamocortical feedforward inhibition in spiny stellate cells is mediated by a small number of fast-spiking interneurons. J Neurosci. 2006; 26:1219–1230. [PubMed: 16436609]

10. Bruno RM, Sakmann B. Cortex is driven by weak but synchronously active thalamocortical synapses. Science. 2006; 312:1622–1627. [PubMed: 16778049]

11. Kremkow J, Perrinet LU, Masson GS, Aertsen A. Functional consequences of correlated excitatory and inhibitory conductances in cortical networks. J Comput Neurosci. 2010; 28:579–594. [PubMed: 20490645]

12. Wang HP, Spencer D, Fellous JM, Sejnowski TJ. Synchrony of thalamocortical inputs maximizes cortical reliability. Science. 2010; 328:106–109. [PubMed: 20360111]

13. Fox K. Anatomical pathways and molecular mechanisms for plasticity in the barrel cortex. Neuroscience. 2002; 111:799–814. [PubMed: 12031405]

14. Foeller E, Feldman DE. Synaptic basis for developmental plasticity in somatosensory cortex. Curr Opin Neurobiol. 2004; 14:89–95. [PubMed: 15018943]

15. Fox K. A critical period for experience-dependent synaptic plasticity in rat barrel cortex. J Neurosci. 1992; 12:1826–1838. [PubMed: 1578273]

16. Shoykhet M, Land PW, Simons DJ. Whisker trimming begun at birth or on postnatal day 12 affects excitatory and inhibitory receptive fields of layer IV barrel neurons. J Neurophysiol. 2005; 94:3987–3995. [PubMed: 16093330]

17. Lee SH, Land PW, Simons DJ. Layer- and cell-type-specific effects of neonatal whisker-trimming in adult rat barrel cortex. J Neurophysiol. 2007; 97:4380–4385. [PubMed: 17392411]

18. Simons DJ, Land PW. Early experience of tactile stimulation influences organization of somatic sensory cortex. Nature. 1987; 326:694–697. [PubMed: 3561512]

19. Stern EA, Maravall M, Svoboda K. Rapid development and plasticity of layer 2/3 maps in rat barrel cortex in vivo. Neuron. 2001; 31:305–315. [PubMed: 11502260]

20. Hull C, Isaacson JS, Scanziani M. Postsynaptic mechanisms govern the differential excitation of cortical neurons by thalamic inputs. J Neurosci. 2009; 29:9127–9136. [PubMed: 19605650]

21. Isaac JT, Oliet SH, Hjelmstad GO, Nicoll RA, Malenka RC. Expression mechanisms of long-term potentiation in the hippocampus. J Physiol Paris. 1996; 90:299–303. [PubMed: 9089495]

22. Maffei A, Nataraj K, Nelson SB, Turrigiano GG. Potentiation of cortical inhibition by visual deprivation. Nature. 2006; 443:81–84. [PubMed: 16929304]

23. Sun QQ. Experience-dependent intrinsic plasticity in interneurons of barrel cortex layer IV. J Neurophysiol. 2009

24. Allen CB, Celikel T, Feldman DE. Long-term depression induced by sensory deprivation during cortical map plasticity in vivo. Nat Neurosci. 2003; 6:291–299. [PubMed: 12577061]

25. Hardingham N, Wright N, Dachtler J, Fox K. Sensory deprivation unmasks a PKA-dependent synaptic plasticity mechanism that operates in parallel with CaMKII. Neuron. 2008; 60:861–874. [PubMed: 19081380]

26. Heynen AJ, et al. Molecular mechanism for loss of visual cortical responsiveness following brief monocular deprivation. Nat Neurosci. 2003; 6:854–862. [PubMed: 12886226]

27. Yoon BJ, Smith GB, Heynen AJ, Neve RL, Bear MF. Essential role for a long-term depression mechanism in ocular dominance plasticity. Proc Natl Acad Sci U S A. 2009; 106:9860–9865. [PubMed: 19470483]

28. Kullmann DM, Lamsa KP. Long-term synaptic plasticity in hippocampal interneurons. Nat Rev Neurosci. 2007; 8:687–699. [PubMed: 17704811]

29. Oren I, Nissen W, Kullmann DM, Somogyi P, Lamsa KP. Role of ionotropic glutamate receptors in long-term potentiation in rat hippocampal CA1 oriens-lacunosum moleculare interneurons. J Neurosci. 2009; 29:939–950. [PubMed: 19176803]

30. Mierau SB, Meredith RM, Upton AL, Paulsen O. Dissociation of experience-dependent and -independent changes in excitatory synaptic transmission during development of barrel cortex. Proc Natl Acad Sci U S A. 2004; 101:15518–15523. [PubMed: 15492224]

31. Philpot BD, Sekhar AK, Shouval HZ, Bear MF. Visual experience and deprivation bidirectionally modify the composition and function of NMDA receptors in visual cortex. Neuron. 2001; 29:157–169. [PubMed: 11182088]

32. Franks KM, Isaacson JS. Synapse-specific downregulation of NMDA receptors by early experience: a critical period for plasticity of sensory input to olfactory cortex. Neuron. 2005; 47:101–114. [PubMed: 15996551]

33. Binshtok AM, Fleidervish IA, Sprengel R, Gutnick MJ. NMDA receptors in layer 4 spiny stellate cells of the mouse barrel cortex contain the NR2C subunit. J Neurosci. 2006; 26:708–715. [PubMed: 16407568]

34. Espinosa F, Kavalali ET. NMDA Receptor Activation by Spontaneous Glutamatergic Neurotransmission. J Neurophysiol. 2009; 101:2290–2296. [PubMed: 19261712]

35. Das S, et al. Increased NMDA current and spine density in mice lacking the NMDA receptor subunit NR3A. Nature. 1998; 393:377–381. [PubMed: 9620802]

36. Al-Hallaq RA, et al. Association of NR3A with the N-methyl-D-aspartate receptor NR1 and NR2 subunits. Mol Pharmacol. 2002; 62:1119–1127. [PubMed: 12391275]

37. Wong HK, et al. Temporal and regional expression of NMDA receptor subunit NR3A in the mammalian brain. J Comp Neurol. 2002; 450:303–317. [PubMed: 12209845]

38. Monyer H, Burnashev N, Laurie DJ, Sakmann B, Seeburg PH. Developmental and regional expression in the rat brain and functional properties of four NMDA receptors. Neuron. 1994; 12:529–540. [PubMed: 7512349]

39. Morishita W, Marie H, Malenka RC. Distinct triggering and expression mechanisms underlie LTD of AMPA and NMDA synaptic responses. Nat Neurosci. 2005; 8:1043–1050. [PubMed: 16025109]

40. Bellone C, Nicoll RA. Rapid bidirectional switching of synaptic NMDA receptors. Neuron. 2007; 55:779–785. [PubMed: 17785184]

41. Feldmeyer D, Egger V, Lubke J, Sakmann B. Reliable synaptic connections between pairs of excitatory layer 4 neurones within a single 'barrel' of developing rat somatosensory cortex. J Physiol. 1999; 521(Pt 1):169–190. [PubMed: 10562343]

42. Petersen CC, Sakmann B. The excitatory neuronal network of rat layer 4 barrel cortex. J Neurosci. 2000; 20:7579–7586. [PubMed: 11027217]

43. Lefort S, Tomm C, Floyd Sarria JC, Petersen CC. The excitatory neuronal network of the C2 barrel column in mouse primary somatosensory cortex. Neuron. 2009; 61:301–316. [PubMed: 19186171]

44. Tamamaki N, et al. Green fluorescent protein expression and colocalization with calretinin, parvalbumin, and somatostatin in the GAD67-GFP knock-in mouse. J Comp Neurol. 2003; 467:60–79. [PubMed: 14574680]

45. Isaac JT, Crair MC, Nicoll RA, Malenka RC. Silent synapses during development of thalamocortical inputs. Neuron. 1997; 18:269–280. [PubMed: 9052797]

46. Agmon A, Connors BW. Thalamocortical responses of mouse somatosensory (barrel) cortex in vitro. Neuroscience. 1991; 41:365–379. [PubMed: 1870696]
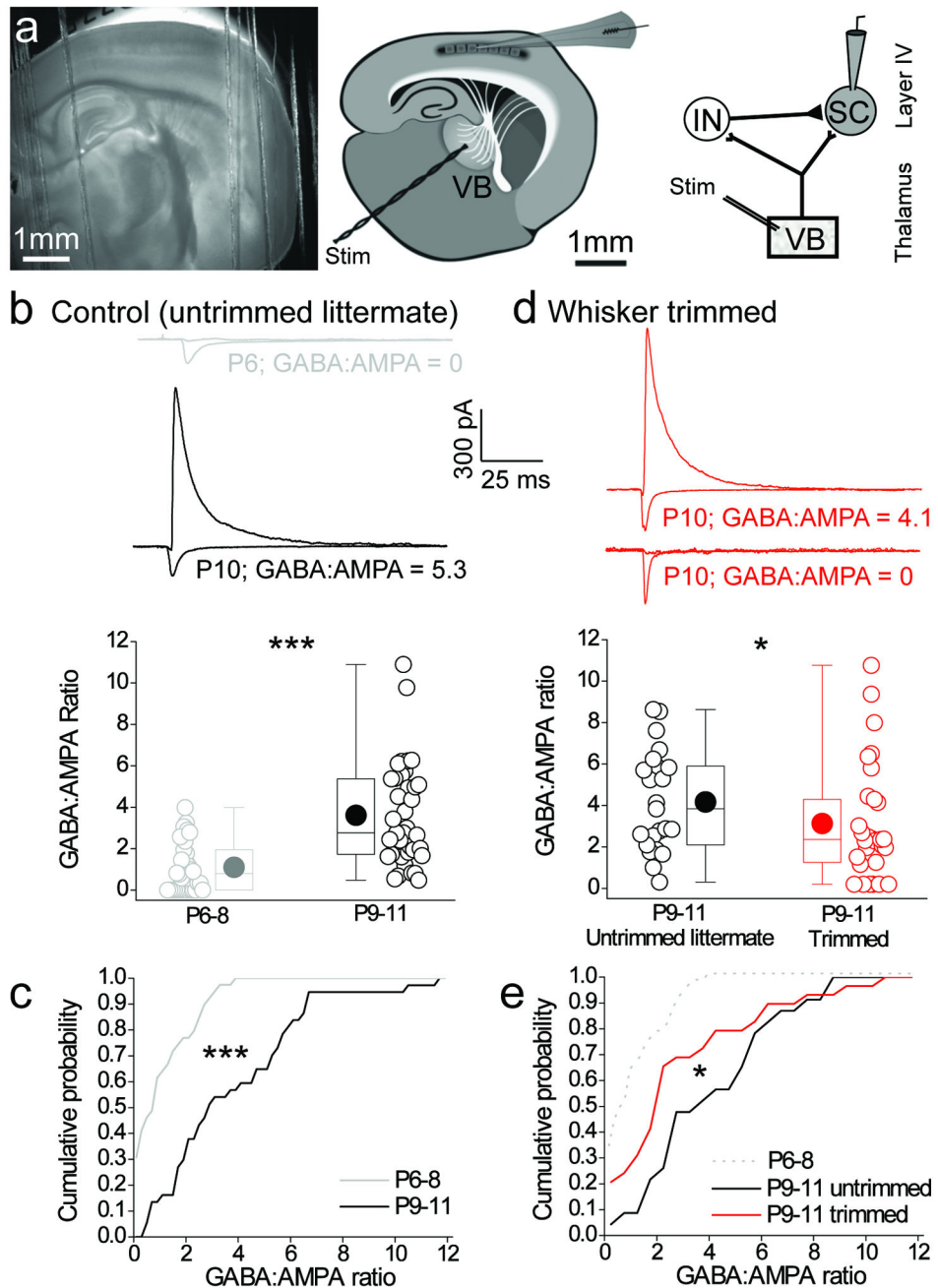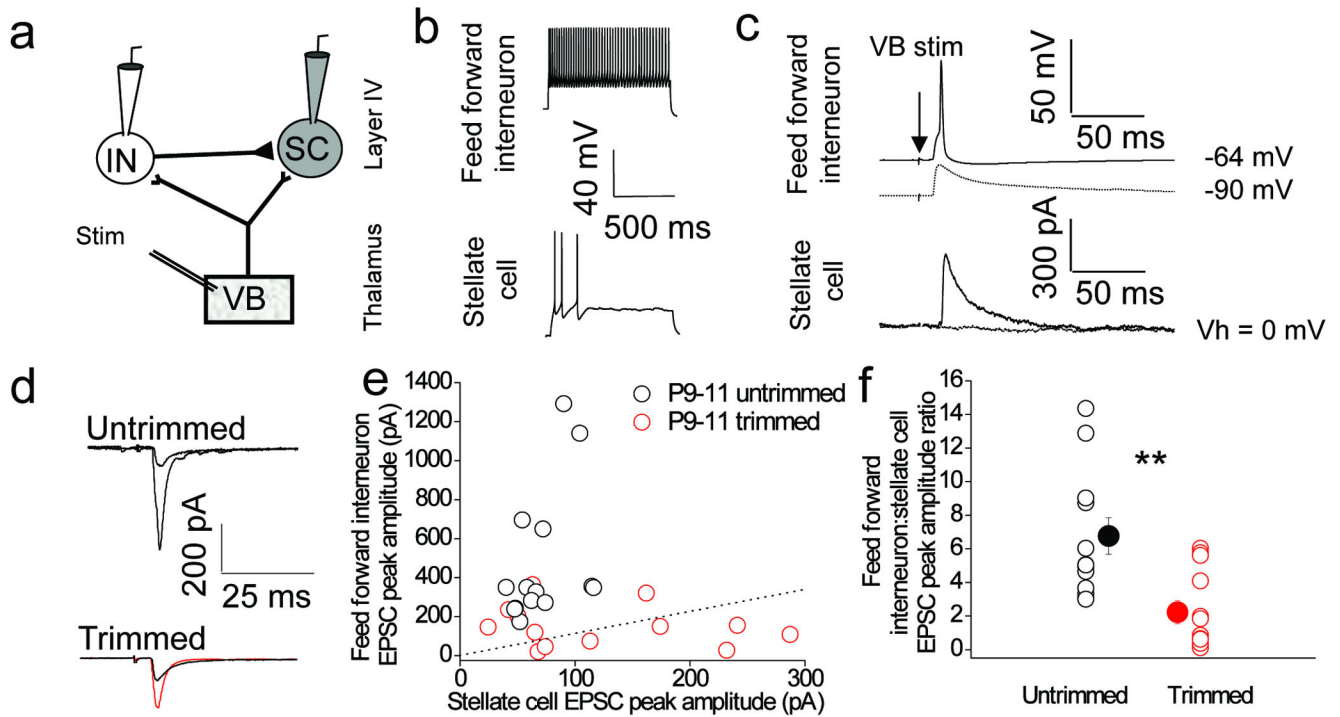
Figure 1. Sensory experience drives the developmental increase in feed–forward inhibitory input in layer 4 barrel cortex

(**a**) 4 × low–magnification DIC image of the thalamocortical slice, (left panel); schematic of the thalamocortical slice indicating placement of the bipolar stimulation electrode in the ventrobasal thalamus (VB) and site of whole–cell recording in layer 4 barrel field (center panel); Schematic of recording configuration depicting stimulation in VB to elicit a monosynaptic excitatory input and disynaptic feed–forward inhibition from the interneuron (IN) to the layer 4 stellate cell (SC; right panel). (**b,c**) Box–and–whisker/scatter plots (see

methods for description) Eroorand cumulative frequency distributions of the amount of feed–forward inhibition calculated as the $GABA_A$:AMPA peak amplitude ratio (GABA:AMPA ratio; see methods for details) during postnatal development for all individual stellate cells recorded and binned for P6–P8 and P9–11 age groups. The voltage clamp traces are from a stellate cell that displayed no feed–forward input at P6 (GABA:AMPA ratio = 0; gray traces) and one with a relatively large GABA:AMPA ratio at P10 (black traces). **(d,e)** Box–and–whisker/scatter plots and cumulative frequency distributions of the GABA:AMPA ratio for all individual stellate cells recorded at P9–11 in whisker–trimmed and untrimmed littermates. Voltage clamp traces are from a stellate cell that displayed a large (GABA:AMPA ratio = 4.1; upper red traces) and no (GABA:AMPA ratio = 0; lower red traces) feed–forward input in P9–11 whisker–trimmed animal. For comparison, the gray dotted line is re–plotted from the P6–8 data in c. n = 23–39. Two tailed Mann–Whitney U–test used for data in b,d and Kolmogorov–Smirnov test used for data in c,e; *p < 0.05, ***p < 0.001.

Figure 2. Sensory experience drives an increase in the relative strength of thalamocortical synaptic transmission onto feed–forward inhibitory interneurons

(a) Schematic of recording configuration depicting stimulation in VB thalamus and simultaneous whole–cell recording from a stellate cell and interneuron in layer 4 barrel cortex. **(b)** Voltage–responses to current injections demonstrating the firing patterns of the interneuron (160 pA injection; upper trace) and stellate cell (40 pA; lower trace). **(c)** Interneurons receiving a monosynaptic VB input capable of eliciting an action potential that is also synaptically connected to the stellate cell (solid traces) were defined as feed–forward interneurons. Hyperpolarizing the feed–forward interneuron resulting in VB input being sub–threshold and completely prevents the feed–forward IPSC measured in the stellate cell (dotted traces). **(d)** Representative voltage clamp traces of thalamocortical EPSCs from a simultaneous feed–forward interneuron and stellate cell recording in P9–11 trimmed and untrimmed littermates. **(e)** Scatter plot of the stellate cell and feed–forward interneuron EPSC peak amplitude relationship in P9–11 trimmed and untrimmed littermates. **(f)** stellate cell and feed–forward interneuron EPSC peak amplitude ratios in P9–11 trimmed and untrimmed littermates. Dotted lines in e and f correspond to EPSC peak amplitude ratio of 1. n = 13–14. Two tailed Mann–Whitney U–test used for data in f, **p < 0.01. Error bars are S.E.M.
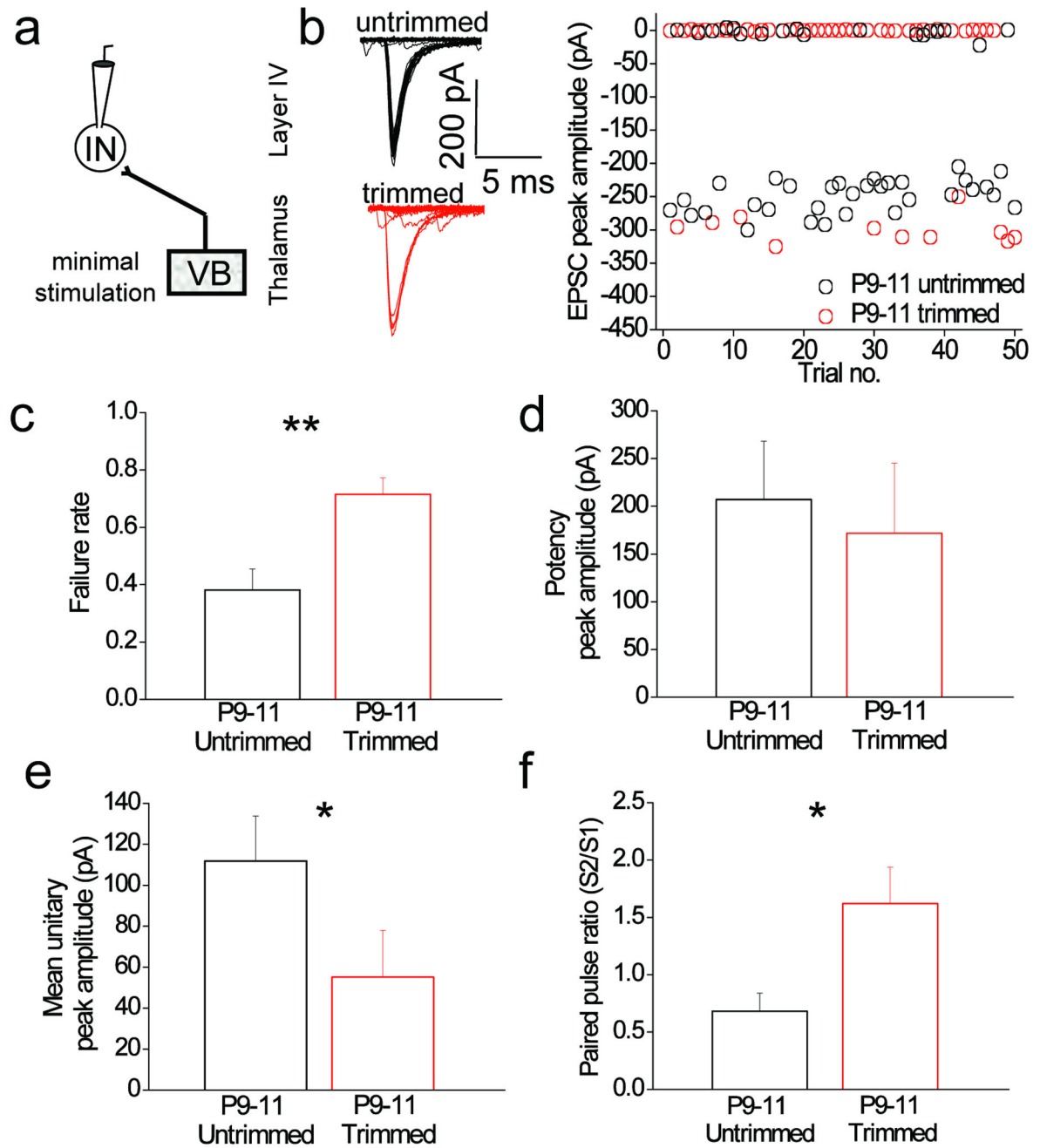
Figure 3. Sensory experience causes a decrease in failure rate and alters paired pulse plasticity at thalamocortical synapses onto feed–forward inhibitory interneurons

(a) Schematic of recording configuration depicting whole–cell recordings from feed–forward intgerneurons in layer 4 barrel cortex. (b) Example traces of unitary thalamocortical EPSCs from feed–forward–interneurons in a P10 untrimmed and a whisker–trimmed littermate evoked via minimal stimulation (see methods). Plot of unitary peak EPSC amplitude from the untrimmed and whisker–trimmed littermate. (c) Failure rate of thalamocortical mediated unitary EPSCs onto feed–forward interneuron in untrimmed and

whisker–trimmed littermates. **(d)** Potency of thalamocortical unitary EPSCs (excluding failures) onto feed–forward interneuron in untrimmed and whisker–trimmed littermates. **(e)** Mean peak amplitudes (including failures) of thalamocortical unitary EPSCs onto feed– forward interneuron in untrimmed and whisker–trimmed littermates. **(f)** Paired pulse ratio (S2/S1) of mean peak amplitudes of thalamocortical unitary EPSCs thalamocortical unitary EPSCs onto feed–forward interneuron in untrimmed and whisker–trimmed littermates. n = 7–8. Two tailed Mann–Whitney U–test used for data in c–f ; *p < 0.05. Error bars are S.E.M.
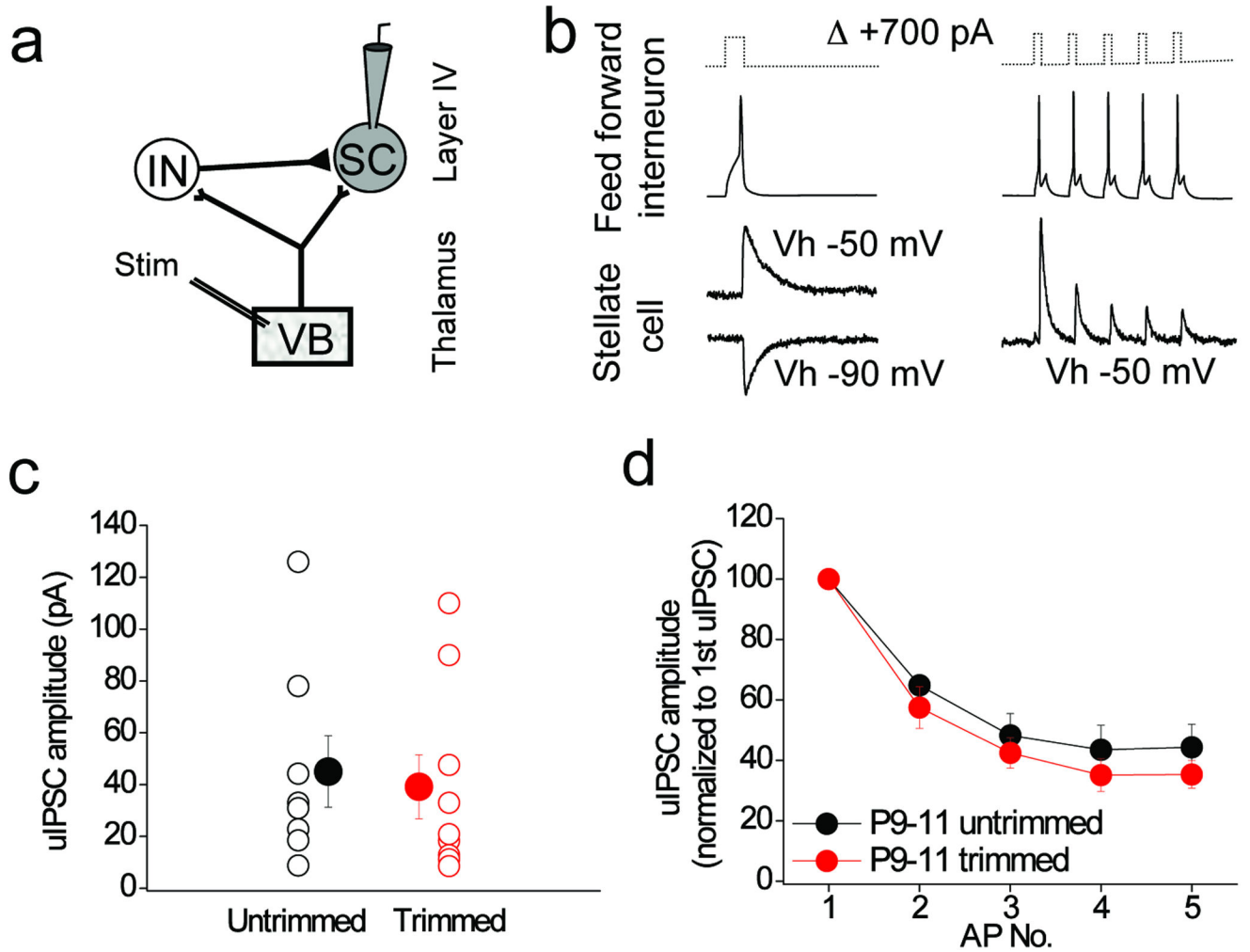
Figure 4. Sensory experience does not alter synaptic transmission or connectivity between feed–forward interneurons and stellate cells in layer 4

(a) Schematic of recording configuration depicting whole–cell recordings from pairs of feed–forward interneurons and stellate cells in layer 4 barrel cortex. **(b)** Example traces demonstrating a connected feed–forward interneuron (action potential elicited by either a single 5 ms, +700 pA current injection, left traces, or 5 action potentials delivered at 50Hz, right traces) and stellate cell pair. The unitary postsynaptic current in the stellate cell is symmetrical around −70 mV as expected from a GABA$_A$–receptor mediated response under the conditions of the experiment. **(c)** Unitary IPSC amplitudes in stellate cells in P9–11 trimmed (n=8) and untrimmed littermates (n=9). Means not significantly different (p > 0.05; two–tailed Mann–Whitney U–test). **(d)** Short term plasticity of feed–forward interneuron to stellate cell unitary IPSCs in P9–11 trimmed (n = 4) and untrimmed littermates (n–5). Error bars are S.E.M.
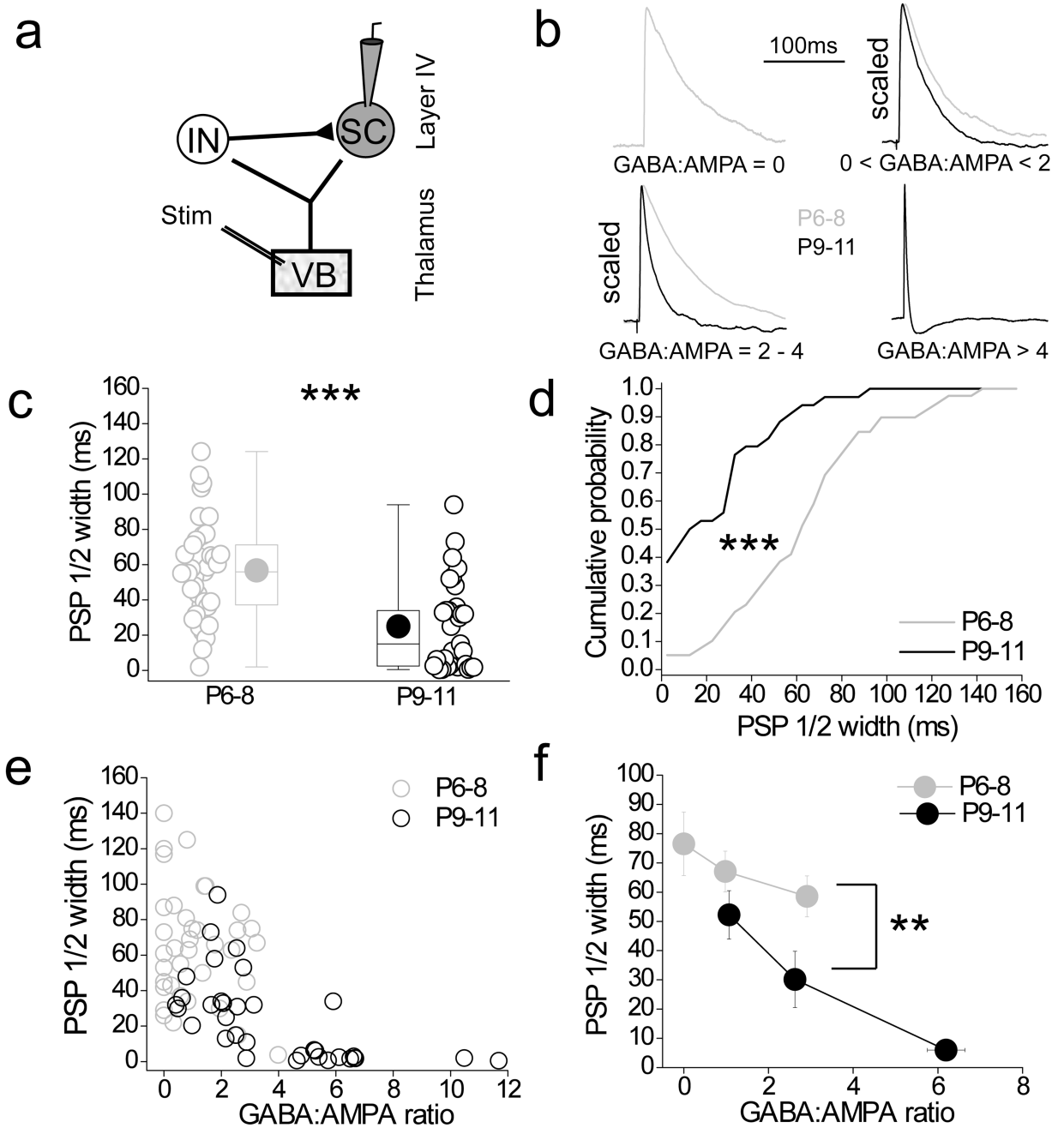
Figure 5. Lack of effective feed–forward inhibition in a subpopulation of stellate cells despite the presence of a relatively large feed–forward inhibitory input

(**a**) Schematic of recording configuration. (**b**) Representative current–clamp traces showing the PSP time–course in stellate cells following VB stimulation. Traces are taken from stellate cells displaying a range of GABA:AMPA ratios as indicated from P6–8 (gray traces) and P9–11 (black traces) age groups. (**c,d**) Box–and–whisker/scatter plots and cumulative distributions of PSP half width at P6–8 (n = 38) and P9–11 (n = 32). (**e**) Correlation plot of GABA:AMPA ratio versus PSP half width for P6–8 (n = 38) and P9–11 (n = 32). (**f**) Pooled
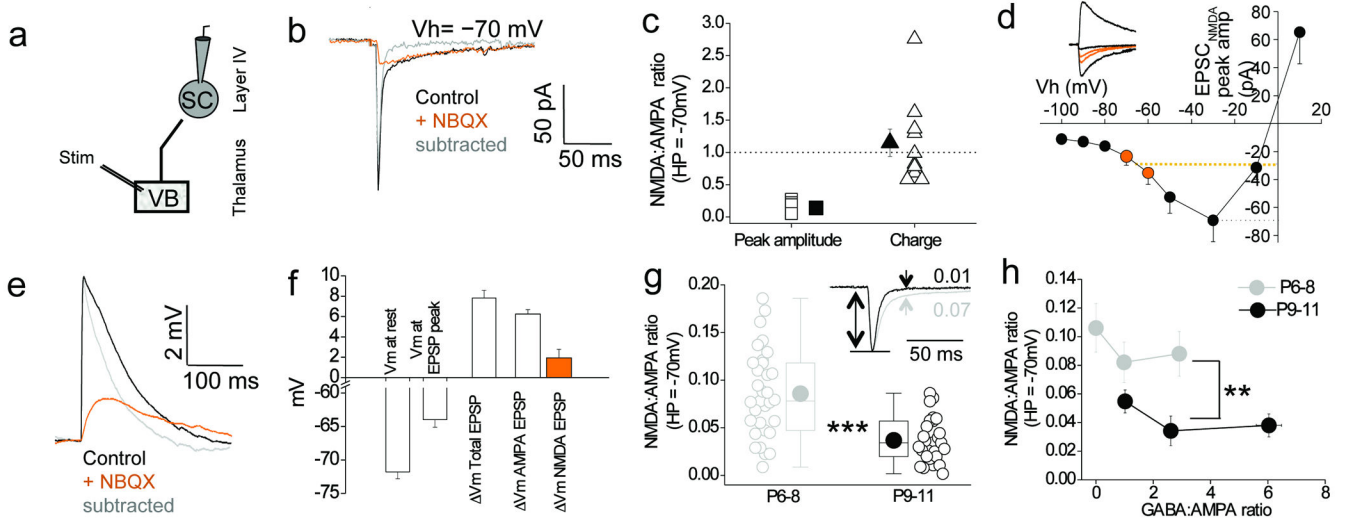
data of the correlation between GABA:AMPA ratio and PSP half width (data were binned according to GABA:AMPA ratios as follows; GABA:AMPA ratio = 0, GABA:AMPA = 0–2, GABA:AMPA ratio = 2–4 and GABA:AMPA ratio > 4; for each data point n = 9–16). Two tailed Mann–Whitney U–test used for data in c, f and Kolmogorov–Smirnov test used for data in d; **p < 0.01, ***p < 0.001. Error bars in (f) are S.E.M.

Figure 6. An NMDA–receptor mediated component to the thalamocortical synaptic response is prominent at resting membrane potential in P6–8 stellate cells and is developmentally down–regulated

(a) Schematic of recording configuration. (b) Representative voltage–clamp traces of the thalamocortical EPSC in a P8 stellate cell at an holding potential (Vh) of −70 mV. (c) Ratio of NMDA:AMPA receptor–mediated peak current amplitude (orange squares) and charge (orange triangles) measured at Vh of −70 mV in P6–8 stellate cells (n=10). Dotted line indicates NMDA:AMPA ratio of 1. (d) Pooled I/V relationship of NMDA EPSC in P6–8 stellate cells (n = 6). Orange dotted line corresponds to the NMDA EPSC peak current amplitude between −60 and −70 mV (closely corresponding to the range of resting potentials measured in P6–8 stellate cells); black dotted line is the maximal NMDA EPSC. Representative traces in inset. For clarity only the EPSC$_{NMDA}$ at −90, −70, −60, −30 and +10 mV are shown. Orange traces are NMDA EPSCs at −60 and −70 mV. (e) Representative thalamocortical EPSPs (P8 stellate cell; resting potential −68 mV). (f) Pooled data for analysis of EPSP in stellate cells (n=6). (g) Box–and–whisker/scatter plots of the NMDA:AMPA ratio at −70 mV for P6–8 (n = 32) and P9–11 (n = 27). Inset: two EPSCs at P6–8 and P9–11. (h) NMDA:AMPA ratio plotted vs. binned GABA:AMPA ratio (same cells as in h). Two tailed Mann–Whitney U–test used for data in g, h; **p < 0.01, ***p < 0.001. Error bars are S.E.M.
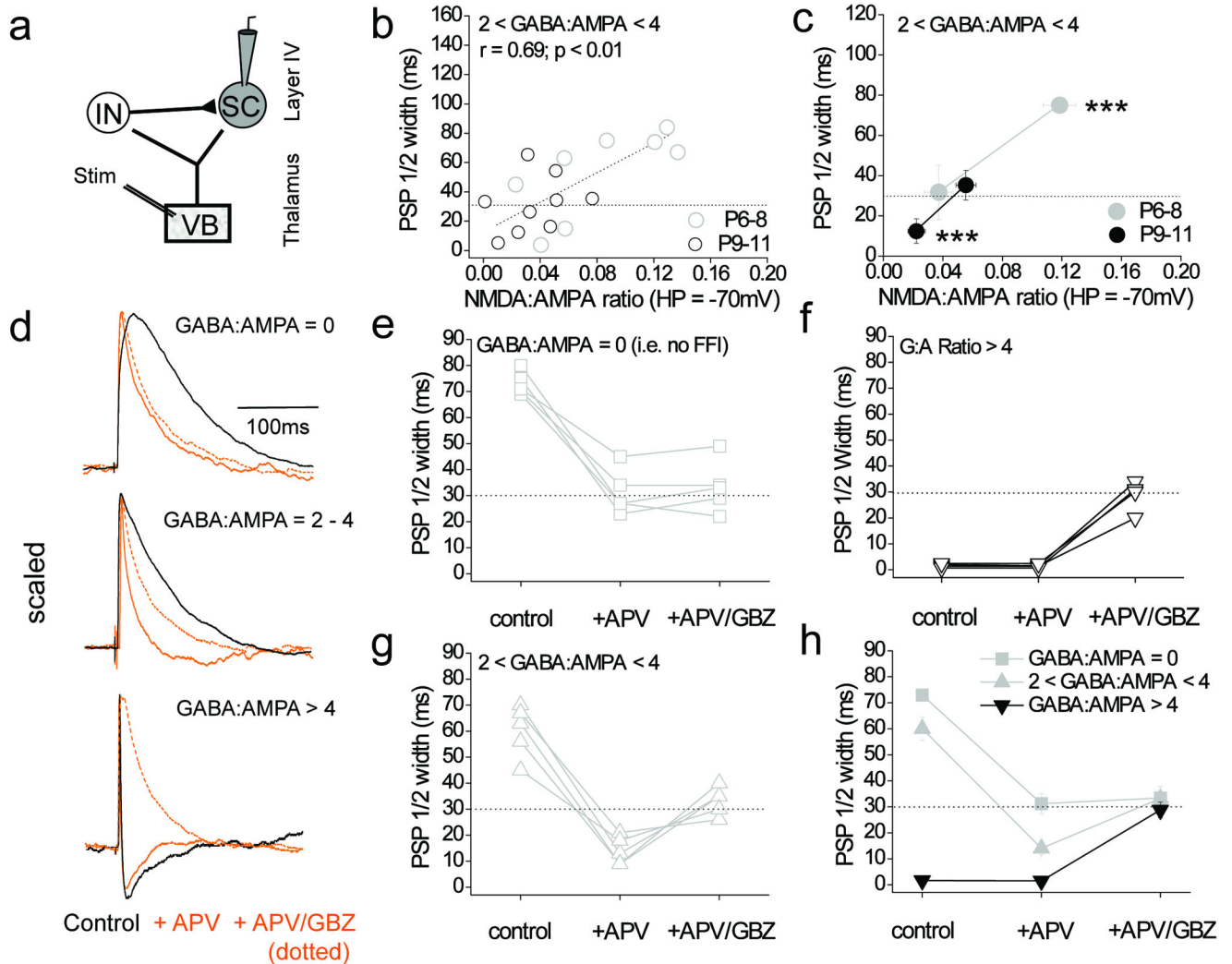
Figure 7. The prominent thalamocortical NMDA component prolongs the PSP to offset the effects of feed–forward inhibiton

(a) Schematic of recording configuration. (b) Scatter plot illustrating a strong correlation in the relationship between NMDA:AMPA ratio (at HP = −70 mV) vs. the PSP half width in stellate cells that display a GABA:AMPA ratio between 2 and 4 for P6-8 (n=8) and P9-11 (n=9). (c) Binned data for the relationship between NMDA:AMPA ratio and PSP half width. *** indicates data points between which both the mean PSP half width and NMDA:AMPA ratio are significantly different to each other (two tailed Mann–Whitney U–test, p < 0.001). (d) Representative traces of pharmacological manipulations as indicated of thalamocortical PSPs in stellate cells with different GABA:AMPA ratios. All EPSPs are scaled to the peak. (e) PSP half widths in P6–8 stellate cells (n = 5) with a GABA:AMPA ratio of 0, in control, in 50 μM APV and in 50 μM APV + 10 μM GBZ. (f) PSP half widths for P9–11 stellate cells (n=4) with a GABA:AMPA ratio > 4 (as for E). (g) PSP half widths for P6–8 stellate cells (n=5) with a GABA:AMPA ratio between 2 and 4 (as for E). (h) Pooled data of the effects of D–APV and D–APV/GBZ application on the PSP half width. Black dotted line in
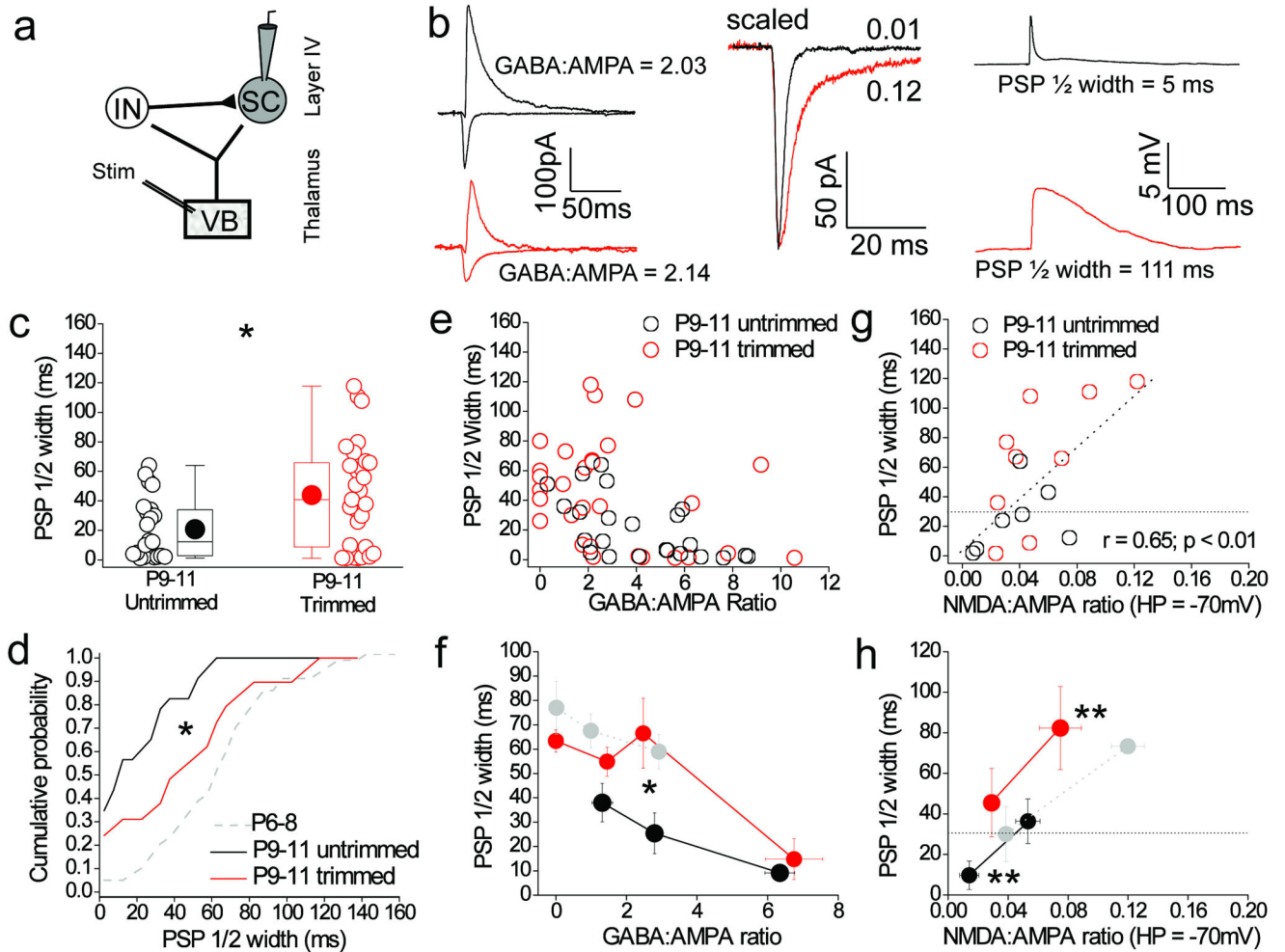
b, c, e–h is half width of the pharmacologically isolated AMPA–receptor mediated thalamocortical EPSP. Error bars are S.E.M.

Figure 8. Sensory experience increases truncation mediated by a given amount of feed forward inhibiton via reduction of the NMDA–receptor mediated component

(a) Schematic of recording configuration. (b) Left panel: voltage clamp traces from two stellate cells in P10 trimmed (red traces) and untrimmed littermate (black traces) displaying very similar GABA:AMPA ratios. Middle panel: close–up of EPSCs (scaled) shown in left panel demonstrating the larger NMDA:AMPA ratio (at HP = −70 mV) in trimmed (red trace) and untrimmed mice (black trace). Right panel: current–clamp traces from the same cells showing the prolonged PSP half width in whisker–trimmed mice. (c,d). Box–and–whisker/scatter plots and cumulative frequency distributions of PSP half widths in all stellate cells tested from trimmed P9–11 (n = 29) and untrimmed littermates (n = 23). Data from same cells as in Figure 1d, e. Gray data from P6–8 re–plotted from Fig. 5d for comparison. (e) GABA:AMPA ratio versus PSP half width for stellate cells in P9–11 trimmed (n = 23) and untrimmed littermates (n = 29). (f) GABA:AMPA ratio vs. PSP half width binned according to GABA:AMPA ratio. Gray data is P6–8 data re–plotted (from Fig. 5f) for comparison. (g) NMDA:AMPA ratio (at HP = −70 mV) vs. PSP half width in stellate cells with a GABA:AMPA ratio between 2 and 4 from P9–11 trimmed (red; n = 9) and untrimmed (black; n = 7) littermates. (h) Binned data of NMDA:AMPA ratio vs. PSP half width in stellate cells with a GABA:AMPA ratio between 2 and 4 in P9–11 whisker–

trimmed (red) and untrimmed littermates (black). ** indicates points between which both the mean PSP half width and NMDA:AMPA ratio are significantly different to each other (two tailed Mann–Whitney U–test, $p < 0.01$). Gray data is P6–8 data re–plotted (from Fig. 6c) for comparison. The black dotted line in g and h is half width of the pharmacologically–isolated AMPA–receptor mediated EPSP. Two tailed Mann–Whitney U–test used for data in c, f, h and Kolmogorov–Smirnov test used for data in d; **$p < 0.01$; *$p < 0.05$. Error bars in (f) and (g) are S.E.M.